A Numerical Study of the Transport and Diffusion of Coastal Pollutants During the Breeze Cycle in the Island of Mallorca

R. Romero C. Ramis

Group of Meteorology, Departament de Fisica, Universitat de les Illes Balears, Palma de Mallorca, Spain

Ann. Geophy., **14**, 351-363 (1996)

Corresponding author address: Dr. Clemente Ramis, Dept. de Fisica, Universitat de les Illes Balears, 07071 Palma de Mallorca, Spain
E-mail: cramis@uib.es

Abstract

An Eulerian study of the distribution over the island of Mallorca of a non-reactive pollutant (SO_2) emitted from an electric power plant operating at present on the north coast is performed using a meso-β numerical model, paying particular attention to the diffusive physical mechanisms. The study is applied to the conditions of sea-land breeze development. This is a local circulation that dominates the flow during the summer and it favors transporting pollutants from the coast toward the centre of the island. Results indicate that values of the ground-level concentration higher than 5 μg/m^3 are restricted over a limited and mountainous region during all the diurnal cycle. However, when the simulation is carried out with the inclusion of a twin electric plant which may be built in the south coast, the affected area becomes larger, specially early in the morning, when the air over the island is sinking as a consequence of the land breeze development. The inclusion of dry deposition in the simulations does not produce important changes in the spatial and temporal evolution of the ground-level concentration.

1 Introduction

Numerical models have been widely used for ambient air quality studies. Since they contain realistic mathematical representations of decisive physical and chemical processes that operate in the atmosphere, such as transport over complex terrain, turbulence, stability-dependent diffusion or transformations by chemical reactions, they can be a practical tool for determining the impact of extant or hypothetical pollutant sources.

For reasons of simplicity, Eulerian models have been often implemented with a two-step process separating the meteorological background and the pollutant transport model. As the first step, direct specification or diagnosis from observations of the wind field over the region of interest is required, as well as quantitative information about diffusive activity. The diffusive activity can be found, for example, by specifying certain stability classes (Pasquill, 1974; Gifford, 1968) which determine the eddy coefficients. In the second step, the meteorological fields are used to solve the conservation relation for the pollutants species (e.g., Davis et al., 1984). With such an approach, simulations of pollutant transport over small and large areas, including complex terrain, have given reasonable results when compared with data of intensive field experiments (King and Bunker, 1984).

Other dispersion models use the meteorological fields already predicted by an operational weather forecasting model and therefore their computation times are low. With such methods, reasonable accuracy has been obtained in cases of large scale atmospheric dispersion of pollutants, as in the case derived from the Chernobyl release (Piedelievre et al., 1990).

However, owing to the structure and diurnal variability of the sea-land breeze (not resolvable by large scale models), plumes from coastal industries and power plants present a complicated behaviour under the influence of this kind of mesoscale circulations. For example, the plume may be swept inland during the sea breeze, rise vertically in the convergence zone and return to the coast transported by the return flow at greater heights (Lyons, 1975), or the plume can drift offshore at night and return to land when the sea breeze develops the next morning. The phenomenon of fumigation in the coastal environment due to strong vertical mixing in the boundary layer also has been recognized as an important agent of ground-level concentration (Hewson and Olsson, 1967). In absence of sufficiently dense (in space and time) meteorological measurements, such complicated behaviour is best treated by means of three-dimensional prognostic models which are able to account for the short-period meteorological variability (e.g., Yamada et al., 1992; Uliasz, 1993; Ferretti et al., 1993). The cost is the large amount of computation time required.

In this work we explore the use of a numerical model in which meteorological fields and pollutant distribution are predicted simultaneously. We apply the model to a situation representing the summer breeze in the island of Mallorca.

The island, located in the centre of the Western Mediterranean, measures approximately 100 x 80 km^2 and possesses three major terrain units: the high relief of the Serra de Tramontana in the west and northwest, with the highest peak of 1440 m; a central lowland plateau; and the eastern uplands of the Serra de Llevant, reaching up to 500 m above sea level. Two big bays are situated in the northeast and the southwest (see Fig. 1).

Meteorological conditions during the summer over the Western Mediterranean normally favor sunshine and fair weather. Moreover, the island is very dry during summer and there is soil water deficit after the beginning of June. These climatological features result in the development, typically from April to October and almost every day during July and August, of the sea breeze in Mallorca. Figure 2, from Jansà and Jaume (1946), shows the main features of the sea breeze in its mature state. The main structure is the convergence line, located in the centre of the island formed by the flux from the two bays. Other convergence zones can be identified, specially in the northeast and the west. On the northwest side of the island the mountain range blocks the current.

The objective of this work is to apply a mesoscale numerical model to study the transport and diffusion during the breeze of non-reactive sulfur dioxide emitted from a power plant located in the north bay of the island (see Fig. 1), paying special attention to the physical mechanisms responsible of the ground-level concentration. The impacts that would result from a potential change in location or magnitude of emissions represent also a subject of applicability of numerical models (e.g. McVehil, 1989, in Alberta, Canada; Hearn, 1989, in Latrobe Valley, Australia). The present study, therefore, is also extended to a future scenario wherein a similar power plant that may be built on the south coast is considered.

The results of two kinds of experiments form the basis of this work. In the first case, dry deposition is not considered. In the second case, dry deposition is included in order to test the sensitivity of the ground-level concentration to this sink process. Prior to the presentation of the results, section 2 gives a brief description of the numerical model and, in section 3, its initialization and the characteristics of the pollutant sources are explained. Results are presented in section 4 and section 5 contains the conclusions.

2 Model description

The primitive equation model used in this work is hydrostatic and three-dimensional. It was developed by Nickerson et al. (1986) and has been used to simulate meso-β circulations (Nickerson et al., 1986; Mahfouf et al., 1987a; 1987b; Pinty et al., 1989; Richard et al., 1989; Romero et al., 1995), and to succesfully simulate the breeze cycle in the island of Mallorca (Ramis and Romero, 1995, hereafter refered to as RR). Further, the same dynamic model has been used in previous dispersion studies (Chaumerliac et al., 1987; Chaumerliac et al., 1992).

In the model, Coriolis force is included. Model equations are expressed in a terrain-following coordinate system, where the vertical coordinate ν is related to the usual σ coordinate by the expression:

$$\sigma = (4\nu - \nu^4)/3$$

The ν coordinate provides for high vertical resolution within the planetary boundary layer (PBL) while at the same time preserving equal spacing between the computational levels.

The energy and water budget equations are applied at the air-soil interface to obtain temperature and moisture at the surface. Diffusion equations for the temperature and moisture content are solved in the soil (Mahfouf et al., 1987a). Solar and infrared fluxes are based on Mahrer and Pielke (1977).

Simultaneously with the prediction of the wind and thermodynamic fields, the model represents the transport and diffusion of pollutants which are assumed not to be affected by chemical reactions. The mean concentration of each chemical species is forecast by the following prognostic equation (see Appendix for a list of symbols):

$$\frac{\partial \pi C_i}{\partial t} = -\frac{\partial \pi C_i u}{\partial x} - \frac{\partial \pi C_i v}{\partial y} - \frac{1}{\sigma'}\frac{\partial \sigma' \pi C_i \dot{\nu}}{\partial \nu} + D_{\pi C_i} + F_{\pi C_i} + S_{\pi C_i}. \quad (1)$$

In this conservation relation, the term $S_{\pi C_i}$ represents the sources and sinks of the pollutant. Neglecting chemical transformations (a constraint that can be accepted for sulfur dioxide released into a dry environment for local studies (McVehil, 1989)) and dry deposition, that term becomes zero except at grid points identified as the contaminant sources.

$D_{\pi C_i}$ and $F_{\pi C_i}$ represent the diffusive terms. The horizontal diffusion $D_{\pi C_i}$ is described by a fourth-order operator. Vertical turbulent mixing $F_{\pi C_i}$ is expressed through an eddy-diffusivity assumption:

$$F_{\pi C_i} = B\frac{\partial}{\partial \nu}\left(BK_{ex}\frac{\partial \pi C_i}{\partial \nu}\right),$$

with

$$B = -\frac{gP}{\pi R_v T \sigma'}.$$

The exchange coefficient K_{ex} is space and time dependent, since it is calculated as a function of the turbulent kinetic energy e, which is predicted by the model, and of the mixing length scale l_k,

$$K_{ex} = 0.4 l_k e^{1/2},$$

following Therry and Lacarrère (1983) and Bougeault and Lacarrère (1989).

3 Initialization and sulfur dioxide sources

There is special interest in studying the environmental impact during the breeze episodes, since the air pollutants released over the coast are easily dragged inland by the current. For that purpose, two numerical simulations were run with identical meteorological background. The first simulation (hereafter S1) includes a sulfur dioxide source that represents continuous emission from the presently working electric plant EP1 (see Fig. 1 for location). In the second simulation (S2), a twin electric plant is added at the point EP2 (see Fig. 1). In both experiments the radiation parameters correspond to 15 July at a latitude of 40^0N. The simulations begin at 0500 LST (on Mallorca, the local time practically matches UTC) and cover the diurnal cycle. The model domain is 150 x 150 km^2 with a horizontal grid length of 2.5 km.

3.1 The atmosphere

We have used 30 vertical levels resulting in 9 computational levels in the lowest kilometre, the first of which is approximately 4.5 metres above the ground. A high resolution of the PBL is important in this kind of simulations. The model has been initialized with a single radiosounding, providing horizontally uniform fields at the beginning of the simulation. This radiosounding (Fig. 3) corresponds to the mean vertical structure of the atmosphere over Mallorca for July at 0000 UTC (Ramis, 1976). During summer, the Azores anticyclone affects the Western Mediterranean. As a consequence of the thermal low-pressure developed over the Iberian peninsula, an anticyclonic circulation becomes reinforced in such manner that the pressure gradient, and therefore the synoptic forcing, is very weak over the Western Mediterranean (Font, 1983). For that reason, the wind has been initialized calm. During the simulation, all fields are relaxed toward their initial values at the lateral boundaries (Davies, 1976).

3.2 The surface

The fluxes at the surface are strongly dependent on the soil texture and moisture, and therefore, hydraulic, thermal and radiative properties of the soil as well as the water content profile must be specified on the land areas. The influence of vegetation, modulated through the shielding factor, is also parameterized by the surface submodel (Pinty et al. 1989).

Figures 4a and 4b show the distribution of soil and vegetation types on the island of Mallorca. Five representative textural classes and vegetative covers have been considered, whose properties and characteristics are summarized in Tables 1 and 2. The shielding factor is low at the centre of the island (< 0.5), but is larger (> 0.5) near the coasts.

The sea surface temperature is 25^0C. The initial temperature on the land surface corresponds to the distribution of the mean minimum temperature during July over the island.

The soil, with a depth of 1 m, is divided into 13 vertical levels. The temperature profile is initially homogeneous, given by the value at the soil surface. Volumetric water content is given as a function of the soil type but is very low near the surface (7-18 % of the saturation value) and increases a little with depth (up to 18-50 % of the saturation value). This profile is typical during summer in Mallorca, since an appreciable water deficit occurs after June. For more details on the surface characteristics, see RR.

3.3 Sulfur dioxide sources

The thermic electric plant burns 2400 T/day of coal with a sulphur content of 0.6 %. The effluents are released into the atmosphere through a stack with a height of 144 m and a diameter of 3.3 m. The gases are released at a temperature of 155 ^{0}C and a vertical velocity of 30 m/s.

For a typical meteorological state during the breeze in Mallorca, those parameters result in an effective source height (Pasquill 1974) of approximately 500 m, which corresponds to the sixth atmospheric level of the computational grid. Further, the nearly constant consumption by the plant results in a continuous emission rate of 0.34 kg/s of SO_2, which is assumed to mix instantly with the environmental air within the source grid cell.

4 Results and discussion

4.1 Meteorological aspects

Prior to the discussion of the pollutant distribution obtained in experiments S1 and S2, a description of the wind field simulated by the model is done. A more complete discussion and verification of the simulated breeze circulation is presented in RR.

The diurnal evolution of the breeze over the island at the lowest level of the model (4.5 m above the ground aproximately) is presented in Fig. 5. At 0900 LST the breeze penetrates inland only a few kilometres except in the northwest coast where the wind is very weak (Fig. 5a). The breeze front is easily identified. The flux is stronger from the two bays, but is more important from the bay of Palma at this time.

The sea breeze reaches its mature state at 1500 LST (shown in Fig. 5b). The wind pattern is very similar to that reported by Jansà and Jaume (1946), shown in Fig. 2. The convergence line formed between the breezes from the two bays is well represented. Other smaller convergence zones are identified in the northeast, close to the coast, in the southeast as a continuation of the main convergence and over the eastern part of the main mountain range. The strongest flux is established from the bay of Alcudia at this time and the blocking action of the Serra de Tramontana can be identified easily. The eastern slope of that mountain range influences the flux from the two bays, which is veering and backing, respectively, toward that warmer slope. Moreover, two small and shallow cyclonic circulations have appeared in the simulation at this time. The first one in the centre of the island as a consequence of the shear between the main currents and the intense sensible heat flux. The second one is located in the west, south of the main mountain group. A vertical cross section along the two bays (Fig. 6a) reveals that the sea breeze has a depth smaller than 1 km. The counter-current, with weaker flow speeds, occupies a vertical depth of about 1 km.

The simulation shows that the sea breeze weakens very quickly after 1900 LST, but those small cyclones persist and have been displaced from their genesis areas. In effect, the wind field at 2100 LST (Fig. 5c) shows that the cyclone previously located in the centre of the island has moved to the north and influences the wind in the bay of Alcudia. At the same time, the western cyclonic circulation has moved to the east and dominates the circulation in the bay of Palma and south coasts.

The surface wind field at the end of the simulation (Fig. 5d) indicates that the circulation has become very weak. However, a land breeze has developed in the southern and eastern parts of the island. A cross section of the thermal structure associated with the mature breeze (Fig. 6b) shows that a dome of superadiabatic lapse rates, and therefore of absolute instability, occupies the centre of the island, with maximum temperatures over the region where the central cyclonic circulation appears.

Given the successful comparisons against observational registers, the meteorological fields supplied by the model can be considered to be a valid approximation to the mean structure of the breeze in Mallorca.

4.2 Ground-level concentration of sulfur dioxide

We have concluded from the experiments that the location of EP1 and EP2 (see Fig. 1), is such that there appears to be no interaction at the ground level between the pollutants released by both plants, at least for this kind of circulation. This means that only the results of experiment S2 are necessary to study the problem. Figure 7 shows the ground-level concentration of sulfur dioxide at the reference times (0900, 1500, 2100 and 0500 LST). The effect of each electric plant can be independently interpreted over the same figure.

The regions of concentrations higher than 5 μg/m^3 are contoured. The main urban sites, located along the bay of Palma, are not affected by the plant emissions. Independently of the values reached, the points of maximum concentration are always at least 5 km away from the sources. The effective height of EP1 and EP2 is widely sufficient to prevent the neighbouring areas from high values of SO_2 concentration.

Analysis of the series of figures showing the temporal evolution of the sea breeze (Fig. 5), shows that the diurnal variability in the circulation around EP1 has two tendencies. In a first stage, the wind initially from the east backs during the morning and becomes northeasterly about 1500 LST. In a second stage, the wind veers; with the arrival of the central cyclone the wind becomes easterly again and, subsequently, with the development of the land breeze, it is from south.

This variability in the wind direction has implications in the transport of air pollutants from EP1. Indeed, the region of concentrations higher than 5 μg/m^3 extends to the west of the electric plant toward the Serra de Tramontana at 0900 LST (Fig. 7a). Later at 1500 LST (Fig. 7b), that region's influence is extended towards the centre of the island, although the convergence line (see Fig. 5b) limits its entrance and deflects the plume toward the mountain range. As the flow veers from northeast to south during the subsequent hours, the region affected by SO_2 moves along the Serra de Tramontana and ends up over the Bay of Pollensa (Figs. 7c and 7d).

It must be noticed that the northern part of the Serra de Tramontana (a wild area), is continually affected by the pollutant as a consequence of its altitude and attraction of the flux from the Bay of Alcudia. From the model results, it seems that the role played by the breeze on the ground concentration of SO_2 emitted by EP1 is not to permit its expansion toward the centre and south of the island, but to restrict its influence on a limited region in the north, mainly mountainous and unpopulated.

In contrast, the behaviour of the wind field in the south around EP2 is simpler. The wind is predominantly southerly during the first hours and veers gradually during the day to become westerly at the decay of the sea breeze (see Fig. 5). As a result, the pollutant extends north to EP2 at 0900 LST (Fig. 7a), but later is transported toward the northeast (Fig. 7b). In this case the pollutant can progress toward the centre and northeast of the island, although such progression is still limited at 1500 LST (Fig. 7b) as a consequence of the convergence line of the eastern part of the island, which tends to deflect the plume toward the central region (see Fig. 5b). However, as the convergence lines disappear and the central cyclonic circulation moves north, the tranport toward the northeast continues.

The maximun SO_2 concentration at the ground also depends on the time, as the mixing layer and advection evolve. At 0900 LST the sea breeze front has not yet penetrated much inland and the winds are light, whereas the vertical diffusion is already appreciable as we will see in next section. As a result, the pollutant released in preceeding hours that has not spread very much, suffers appreciable vertical mixing and values higher than 40 μg/m^3 for EP1 and 45 μg/m^3 for EP2 occur at the ground (see Fig. 7a).

At 1500 LST the breeze is in its mature state (wind speeds stronger than 8 m s^{-1} occur in the bay of Alcudia). The flux reaches the centre of the island and a deep mixing layer develops there. Strong vertical mixing in a deeper and wider region leads to lower values of the concentration at the ground (Fig. 7b).

From that time, the breeze and turbulent mixing weaken progressively but horizontal diffusion continues. As a result, ground concentrations derived from EP2 are smaller than 5 μg/m^3 at 2100 LST. However, the pollutant from EP1 is blocked over the eastern slope of the Serra de Tramontana and values higher than 20 μg/m^3 are given by the model at that time (Fig. 7c).

During the sunshine hours, vertical diffusive mechanisms are the main factors in the ground-level concentration pattern. However, after sunset, vertical diffusion plays a secondary role, whereas the transport by downward air motion over the island associated with the land breeze becomes the dominant mechanism. A substantial increase of the sulfur dioxide at low levels is produced as a consequence of this transport process. That effect can be seen at 0500 LST (Fig. 7d). The sulfur dioxide from EP1 maintains its concentration over lowlands about the bay of Pollensa. That released from EP2 which remained in upper levels has sunk spectacularly, and practically all the eastern side of the island has concentrations exceeding 10 μg/m^3.

From the point of view of the regulated ambient air quality standards, the concentrations forecast by the model are appreciably smaller than those characteristic of a very polluted area. For example, the daily average value of 130 μg/m^3, which is the upper limit established by the spanish government, is not exceeded at any point on the island according to the model results.

4.3 Vertical cross sections

A series of vertical cross sections have been included and discussed in order to support some results commented in last section. Vertical diffusion has been identified, except in the night, as the main factor in the ground concentration intensity. During the initial hours, when the winds are still light and restricted over the coastal areas, the vertical diffusion over land is already appreciable, although the mixing layer depth is moderated. That leads to fumigation and high values of ground-level concentration not too far from the coast. Later, as the cold air from the sea penetrates inland with a well defined sea breeze, vertical turbulent diffusion diminishes near the coast but intensifies and extends vertically toward the centre of the island, where strong sensible heat flux occurs. Therefore, the fumigation moves inland, although the mixing acts in a deeper layer and lower values of the concentration are reached at the ground. This behaviour of the vertical diffusion is shown clearly in Fig. 8, which represents the turbulent kinetic energy in a cross section along the bays of Palma and Alcudia (see Fig. 1 for location). At 0900 LST, turbulent diffusivity exceeding 1 m^2/s^2 is restricted to below a height of 1 km, but is very homogeneous over great part of the island (Fig. 8a). At 1500 LST, turbulent diffusivity has fallen by one half near the coasts, specially near the bay of Alcudia, but has doubled over the centre of the island and occupies a height of 1.5 km (Fig. 8b).

As was pointed out in last section, as the incoming radiation decreases late in the day, the vertical diffusion loses its activity and low values of SO_2 occur at the ground (except around EP1 due to the blocking action of the Serra de Tramontana). This effect can be seen in Fig. 9, which shows a cross section of the sulfur dioxide concentration at 2100 LST along the direction AB (indicated in Fig. 1), for the experiment S1. The pollutant is confined against the eastern slope of the mountain range.

The interaction with the orography is not as important in the case of EP2 since the terrain is not as complex and elevated in the east of the island. The extensive impact of EP2 is well reflected in the cross sections contained in Fig. 10, which corresponds to the sulfur dioxide concentration along the direction CD (indicated in Fig. 1), for the experiment S2. At 0900 LST, concentrations higher than 5 μg/m^3 exist only in the proximity of the coast below a height of 900 m (Fig. 10a). However, with the mature breeze at 1500 LST, that region extends its influence to almost the opposite coast and has a vertical mixing depth of 2 km, producing smaller values at ground-level (Fig. 10b). The dome observable in the centre of the figure could be attributed to the transport by the upward air motion over the convergence zone. On the other hand, the figure shows that the pollutant is also transported backward by the counter-current over the source level. Figure 10c shows that, as mentioned in the last section, the pollutant remains about at the source level and does not affect the ground during the night. An examination of the wind field at source level during the nocturnal hours (not shown), reveals that a slight transport from C to D exists all this time. With the land breeze established during the early morning, the pollutant is forced to descend over the land as the air does, and the concentration at ground-level increases again, although affecting a larger region (see Fig. 10d).

4.4 Comparison against sampler data

The disposition of permanent SO_2 measurements in Mallorca is very limited and is not sufficient to permit a detailed comparison with the model results. The measurements also are affected by local features not resolvable by the model. Moreover, as a consequence of the initialization data, the meteorological fields given by the model suppose an approximation to the mean structure of the breeze and not to the circulation of any particular day. Small differences in wind direction, for example, can produce a large difference in computed and measured concentration sufficiently downwind of a source (King and Bunker 1984).

Unfortunately, measurements in the region where the model indicates the highest concentrations of sulfur dioxide from EP1 do not exist at present. The available station IE1 (see Fig. 1 for location) is located near the boundary of the area with appreciable pollutant concentration shown by the model (see Fig. 7).

Figure 11 shows the graphical comparison at the station IE1 with observations on

27 and 28 July 1993, when a sea breeze developed. The order of magnitude of the concentration is well represented by the model throughout the diurnal cycle. Even the shape of the curves, dominated by the maximum between 0900 and 1300 LST, is well simulated by the model. A secondary maximum given by the model at 2300 LST, is also reflected in the data of one of the days.

4.5 Impact of dry deposition

In the previous experiments, dry deposition was not considered. This sink process can be neglected for species that do not undergo chemical reaction at the surface or that are insoluble in water; for example carbon monoxide. However, SO_2 is highly water-soluble and therefore behaves similarly to water vapour, exhibiting deposition velocities of up to $1\ \mathrm{cm\,s^{-1}}$ (Sehmel, 1980).

Although the physical mechanisms governing the behaviour of the coastal pollutants seem clear from the previous simulations, it is worthwhile to examine the modification of ground-level concentration when dry deposition of SO_2 is included in the model. For that purpose, we have repeated the experiment S2 (in this case covering two diurnal cycles) but with the deposition flux $v_d \pi C_i$ as the lower boundary condition in the conservation equation (1).

The deposition velocity v_d is calculated in terms of a total resistance $r_a + r_{na}$ (Wesely and Hicks, 1977):

$$v_d = (r_a + r_{na})^{-1}$$

The atmospheric resistance r_a is given as

$$r_a = (ku_*)^{-1} \left[\ln\left(\frac{z_s}{z_0}\right) - \Psi \right]$$

where k is the Von Karman constant, u_* the friction velocity, z_s the reference height and z_0 the roughness length. Ψ is the stability correction factor, which is approximated as

$$\Psi = \begin{cases} \exp[0.598 + 0.39\ln(-z_s/L) - 0.09\ln^2(-z_s/L)], & -1 < z_s/L < 0 \\ 0, & z_s/L = 0 \\ -5z_s/L, & 0 < z_s/L < 1 \end{cases}$$

where L is the Monin-Obukhov length.

Over the sea, the nonatmospheric resistance r_{na} for SO_2 is approximated by $1/u$ (Slinn et al., 1978), where u is the mean surface wind predicted by the model. Over land areas, r_{na} is composed by the deposition layer resistance (r_d) and the canopy/vegetation resistance (r_c). Following Wesely and Hicks (1977), r_d is given by the expression

$$r_d = 2.5/ku_*$$

For gases such as SO_2, the canopy resistance r_c is dominated by the stomatal resistance which is calculated by the surface sub-model as function of the vegetation type (minimum values are given in Table 2).

The results for the first diurnal cycle reveal that the effect of dry deposition on ground-level values can be only clearly discerned at 1500 LST, with reductions of up to 5 μg/m^3 in some areas (compare Fig. 12 against Fig. 7b). This fact is consistent with the highest deposition velocities reached at that time over the centre of the island where the thermal stability is weak.

An important issue is the effect of a second cycle of breeze on the pollutant distribution. The results of the second cycle practically reproduce the patterns found in the first diurnal period except at 0900 LST. At that time (Fig. 13), the SO_2 transported inland during the night is still present at low levels while a new fumigation process has started. With such conditions, much of the centre of the island is affected by the pollutant and there is interaction between the pollutants released from EP1 and EP2 (compare Fig. 13 against Fig. 7a).

It should be noted, however, that the absence of chemical transformations becomes more critical as the simulation time increases. Furthermore, the accumulation of pollutants in the island environment is a direct consequence of the initial and boundary conditions, which are somewhat artificial since the slight transport associated with the synoptic winds (typically weak during summer as was indicated in section 3.1) has been totally supressed in the initialization process. In fact, as discussed in RR, the simulated meteorological fields must be only considered as the mean circulation of the breeze. Really, when the synoptic flow is important enough, the actual breeze can be enhanced, reduced or modified significantly.

5 Conclusions

A numerical study of the pollutant transport and diffusion over the island of Mallorca based on two numerical simulations has been presented. The study has focused in a particular meteorological situation, very common during the summer season, and the most favourable for capturing the pollutants emitted by coastal sources over the island. Such circulation is the breeze, which has already been simulated and discussed in Ramis and Romero (1995).

The simulations cover a diurnal cycle and, therefore, the winds and stability are highly variable throughout the simulation, affecting continously the advection and diffusion of the pollutant. In order to capture such dependence better, meteorological and pollutant conservation equations are simultaneously solved by the numerical model. Moreover, vertical diffusion is calculated as function of the turbulent kinetic energy, also predicted by the model.

In the first simulation, the effluence of non-reactive sulfur dioxide from a real power plant located in the north bay of the island is considered. The convergence line along the centre of the island limits the plume expansion toward the south and deflects its transport toward the Serra de Tramuntana (the major wild area of the island), which acts to block the pollutant. During the night, the plume moves along the Serra de Tramuntana and finally concentrates about the shore when a new sea breeze begins its development. The simulation reveals that, during all the diurnal cycle, the region of ground-level concentration higher than 5 μg/m^3 is small. Such a region is not covered by the current measurements and therefore the model accuracy cannot be entirely validated.

A second simulation is performed in order to assess the impact of the power plant system that will probably work in the island in the next future. Thus, an identical sulfur dioxide source has been added on the south coast. The results show that there is no interaction at low levels between the pollutants from both plants, and that the main urban sites located in the south bay of the island remain unaffected. Again, the convergence zones intercept the transport of the new plume towards the north, but in this case the plume can progress much further inland and this progression continues during the night after the decay of the sea breeze. Vertical diffusion proves to be the main factor in the ground-level concentration intensity during the day, leading to high values in the morning due to appreciable diffusion over the whole island, and lower values in the afternoon as the mixing layer weakens near the coast but intensifies in the centre of the island. However, after the decay of the breeze, fumigation to ground stops and the downward air motion related with a slight land breeze becomes the process most responsible for the ground-level concentration at the beginning of the next cycle. In this sense, the impact of the new power plant seems to be more important, since practically all the eastern part of the island is affected by the pollutant sinking. Another simulation including the dry deposition flux reveals that this process is not important to define the intensity of the ground-level concentration except during the central part of the day.

This study could help to improve the present disposition of pollutant measurement sites and to improve the design of a future sampling network for air quality control in Mallorca. At the same time, this work could be taken as a reference point to continue the discussion about the impact of future coastal power plants and industries on small islands.

Acknowledgements. The authors gratefully acknowledge the assistance of Dr. M. Colom (Environmental Agency of the Regional Government) for providing the SO_2 concentration data used in this work. The authors also thank Dr. J. Vadell (Department of Environmental Biology, UIB) for his help in the determination of the surface characteristics of Mallorca and Dr. S. Alonso for his valuable suggestions during the development of this study. This work has been partially supported by CE EV5V-CT94-0442 grant.

APPENDIX

List of Symbols

B	vertical scale factor given by $B = -\frac{gP}{\pi R_v T \sigma'}$
C_i	concentration of the chemical substance (mass/mass)
$D_{\pi C_i}$	horizontal difussion term
e	turbulent kinetic energy
$F_{\pi C_i}$	turbulent mixing term
g	acceleration of gravity
k	Von Karman constant
K_{ex}	exchange coefficient
L	Monin-Obukhov length
l_k	turbulent mixing length
P	pressure
P_s	surface pressure
P_t	pressure at the upper boundary = 100 hPa
r_a	atmospheric resistance
r_c	canopy/vegetation resistance
r_d	deposition layer resistance
r_{na}	nonatmospheric resistance
R_v	universal gas constant
$S_{\pi C_i}$	source-sink terms
t	time
T	temperature
u	wind component along the x-direction
u_*	friction velocity
v	wind component along the y-direction
v_d	dry deposition velocity
x	coordinate in the west-east direction
y	coordinate in the south-north direction
z_0	roughness length
z_s	reference height
π	$(P_s - P_t)$
σ	pressure coordinate defined by $\sigma = (P - P_t)/\pi$
σ'	$d\sigma/d\nu$
ν	vertical coordinate related with σ by $\sigma = (4\nu - \nu^4)/3$
$\dot{\nu}$	vertical velocity

REFERENCES

Bougeault, P. and P. Lacarrère, Parameterization of orographic induced turbulence in a mesobeta scale model, *Mon. Wea. Rev.,* **117,** 1872-1890, 1989.

Chaumerliac, N., E. Richard, J. P. Pinty and E. C. Nickerson Sulfur scavenging in a mesoscale model with quasi-spectral microphysics: Two-dimensional results for continental and maritime clouds, *J. Geophys. Res.*, **92,** 3114-3126, 1987.

Chaumerliac, N., R. Rosset, M. Renard and E. C. Nickerson The transport and redistribution of atmospheric gases in regions of frontal rain, *J. Atmos. Chemistry,* **14,** 43-51, 1992.

Clapp, R. and G. Hornberger, Empirical equations for some soil hydraulic properties, *Water Resour. Res.*, **14,** 601-604, 1978.

Davies, H. C., A lateral boundary formulation for multilevel prediction models, *Quart. J. R. Meteor. Soc.,* **102,** 405-418, 1976.

Davis, C. G., S. S. Bunker and J. P. Mutschlecner, Atmospheric transport models for complex terrain, *J. Climate Appl. Meteor.,* **23,** 235-238, 1984.

Ferretti, R., G. Visconti and F. Giorgi, Chemistry and transport of sulphur compounds from large oil fires studied with a 2D mesoscale model, *Ann. Geophy.,* **11,** 68-77, 1993.

Font, I., *Climatología de España y Portugal,* Instituto Nacional de Meteorología, Madrid, 1983.

Gifford, F., *An outline of theories of diffusion in the lower layers of the atmosphere,* Meteorology and Atomic Energy, H. Slade Ed., 65-116, 1968.

Hearn, D., *ISC modelling of sulfur dioxide concentrations in the Latrobe valley,* In Man and his Ecosystem. Brasser L. J. and Mulder W.C. editors, Elsevier Sci. Publ., 269-273, 1989.

Hewson, E. W. and L. E. Olsson, Lake effects on air pollution dispersion, *J. Air Poll. Cont. Assoc.,* **17,** 757-761, 1967.

Jansà, J. M. and E. Jaume, The sea breeze regime in the Mallorca island (in spanish), *Rev. de Geofísica,* **19,** 304-328, 1946.

King, D. S. and S. S. Bunker, Application of atmospheric transport models for complex terrain, *J. Climate Appl. Meteor.,* **23,** 239-246, 1984.

Lyons, W. A., *Turbulent diffusion and pollutant transport in shoreline environments,* In D. Haugen ed., Lectures on Air Pollution and Environmental Impact Analyses, Boston: American Meteorological Society, 1975.

Mahfouf, J. F., E. Richard and P. Mascart, The influence of soil and vegetation on the development of mesoscale circulations, *J. Climate Appl. Meteor.,* **26,** 1483-1495, 1987a.

Mahfouf, J. F., E. Richard, P. Mascart, E. C. Nickerson and R. Rosset, A comparative study of various parameterizations of the Planetary Boundary Layer in a numerical mesoscale model, *J. Climate Appl. Meteor.,* **26,** 1671-1695, 1987b.

Mahrer, Y. and R. A. Pielke, The effects of topography on the sea and land breezes in a two-dimensional numerical model, *Mon. Wea. Rev.,* **105,** 1151-1162, 1977.

McCumber, M. C., *A numerical simulation of the influence of heat and moisture fluxes upon mesoscale circulations,* Ph. D. dissertation, University of Virginia, 255 pp, 1980.

McVehil, G. E., *Model estimates of provincial scale atmospheric sulphur dioxide (SO_2) and oxides of nitrogen (NO_x) in Alberta,* In Acidic deposition: Sulphur and nitrogen oxides. Legge A. H. and Krupa S. U. editors, CRC Press, Inc., 433-475, 1989.

Nickerson, E. C., E. Richard, R. Rosset and D. R. Smith, The numerical simulation of clouds, rain and airflow over the Vosges and Black forest mountain: a meso-β model with parameterized microphysics, *Mon. Wea. Rev.,* **114,** 398-414, 1986.

Pasquill, F., *Atmospheric Diffusion,* 2nd ed., Wiley & Sons, 429 pp., 1974.

Piedelievre, J. P., L. Musson-Genon and F. Bompay, MEDIA-An eulerian model of atmospheric dispersion: First validation on the Chernobyl release, *J. Appl. Meteor.,* **29,** 1205-1220, 1990.

Pinty, J. P., P. Mascart, E. Richard and R. Rosset, An investigation of mesoscale flows induced by vegetation inhomogeneities using an evapotranspiration model calibrated against HAPEX-MOBILHY data, *J. Appl. Meteor.,* **28,** 976-992, 1989.

Ramis, C., *Climatology of the upper air over Mallorca (in spanish),* Univ. de Barcelona, 66 pp., 1976.

Ramis, C. and R. Romero, A first numerical simulation of the development and structure of the sea breeze in the island of Mallorca, *Ann. Geophy.,* 1995. (in press).

Richard, E., P. Mascart and E. C. Nickerson, The role of surface friction in downslope windstorms, *J. Appl. Meteor.,* **28,** 241-251, 1989.

Romero, R., S. Alonso, E. C. Nickerson and C. Ramis, The influence of vegetation on the development and structure of mountain waves, *J. Appl. Meteor.,* **34,** 2230-2242, 1995.

Sehmel, G. A., Particle and gas dry deposition: A review, *Atmos. Environ.,* **14,**

983-1011, 1980.

Slinn, W. G. N., L. Hasse, B. B. Hicks, A. W. Hogan, D. Lal, P. S. Liss, K. O. Munnich, G. A. Sehmel and O. Vittori, Some aspects of the transfer of atmospheric trace constituents past the air-sea interface, *Atmos. Environ.,* **12,** 2055-2087, 1978.

Therry, G. and P. Lacarrère, Improving the eddy-kinetic energy model for planetary boundary layer description, *Bound. Layer Meteor.,* **25,** 63-88, 1983.

Uliasz, M., The atmospheric mesoscale dispersion modeling system, *J. Appl. Meteor.,* **32,** 139-149, 1993.

Wesely, M. L. and B. B. Hicks, Some factors that affect deposition rates of SO_2 and similar gases on vegetation, *J. APCA,* **27,** 1110-1116, 1977.

Yamada, T., S. Bunker and M. Moss, Numerical simulations of atmospheric transport and diffusion over coastal complex terrain, *J. Appl. Meteor.,* **31,** 565-578, 1992.

Soil type	η_s	K_{η_s} ($.10^{-6}$ m s^{-1})	ψ_s (m)	$\rho_i c_i$ ($.10^{6}$ J m^{-3} K^{-1})	b	ε	a	z_0 (mm)
Sand	0.395	176.0	-0.121	1.463	4.05	0.99	0.25	5
Sandy Loam	0.410	156.0	-0.090	1.404	4.38	0.99	0.25	5
Silt Loam	0.430	25.0	-0.200	1.300	4.80	0.99	0.30	5
Clay Loam	0.460	3.0	-0.440	1.150	8.40	0.99	0.25	5
Clay	0.482	1.3	-0.405	1.089	11.40	0.99	0.35	5

Table 1: Soil parameters for five textural classes representative of Mallorca. The parameters have been computed by combining those given in the classification of the U. S. Department of Agriculture (Clapp and Hornberger, 1978; McCumber, 1980): η_s (soil porosity), K_{η_s} (saturated hydraulic conductivity), ψ_s (saturated moisture potential), $\rho_i c_i$ (dry volumetric heat capacity) and b (dimensionless exponent). ε is the emissivity, a the albedo and z_0 the roughness length.

Parameter	Vegetation type				
	Tall Grass	**Shrub**	**Crop**	**Conifer Forest**	**Woodland**
Height (m)	2.0	0.5	0.4	12.0	10.0
Displacement height (m)	1.50	0.37	0.30	9.00	7.50
Plant resistance (s)	8.10^9	10.10^9	6.10^9	8.10^9	8.10^9
Minimum stomatal resistance (s m^{-1})	350	500	50	350	350
Critical leaf water potential (m)	-150	-150	-100	-150	-180
Green leaf area index	2.0	1.0	1.0	3.5	5.0
Dry leaf area index	2.0	2.0	0.1	0.7	1.0
Canopy emissivity	0.98	0.98	0.96	0.98	0.98
Canopy albedo	0.16	0.16	0.20	0.10	0.15
Roughness length (m)	0.17	0.04	0.03	1.00	0.83
Average rooting depth (m)	0.2	0.2	0.2	0.9	0.9

Table 2: Parameters of five representative types of vegetation of Mallorca. The values have been approximated using the HAPEX-MOBILHY data (Pinty et al., 1989).

FIGURES

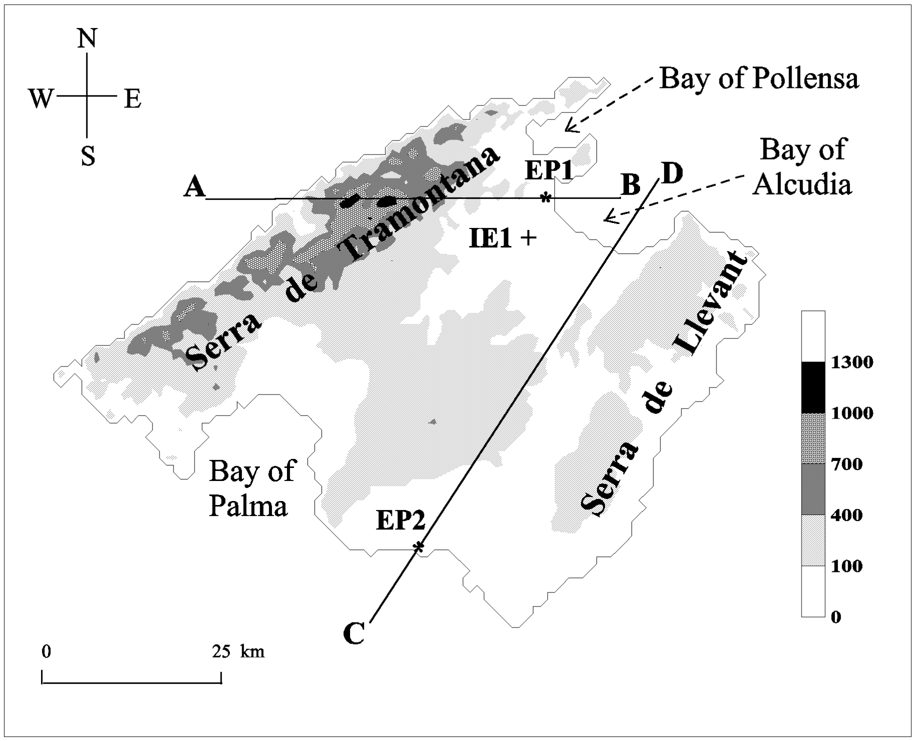

Figure 1: The island of Mallorca. Orography and the sites referred in the text are indicated. EP1 and EP2 represent the electric power plants (*), whereas IE1 represents the pollutant concentration measurement site (+). AB and CD indicate the cross-sections discussed in the text.

Figure 2: Streamlines of the mature sea breeze over Mallorca (from Jansà and Jaume 1946; reproduced by permission of Rev. de Geofísica).

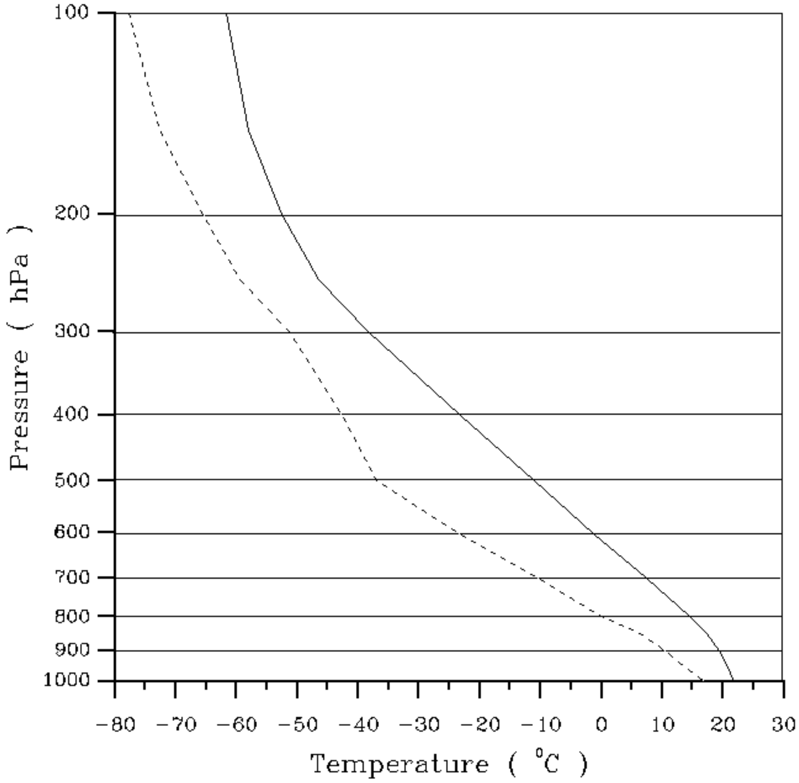

Figure 3: Mean vertical structure of the atmosphere over Mallorca in July at 0000 UTC (after Ramis, 1976). Solid line represents temperature and dashed line represents dew point.

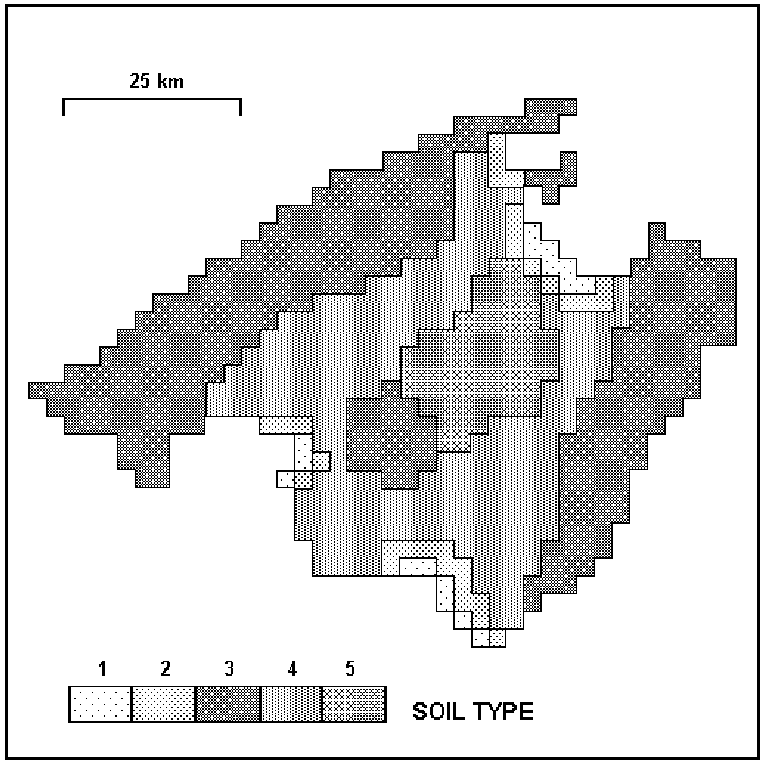

(a)

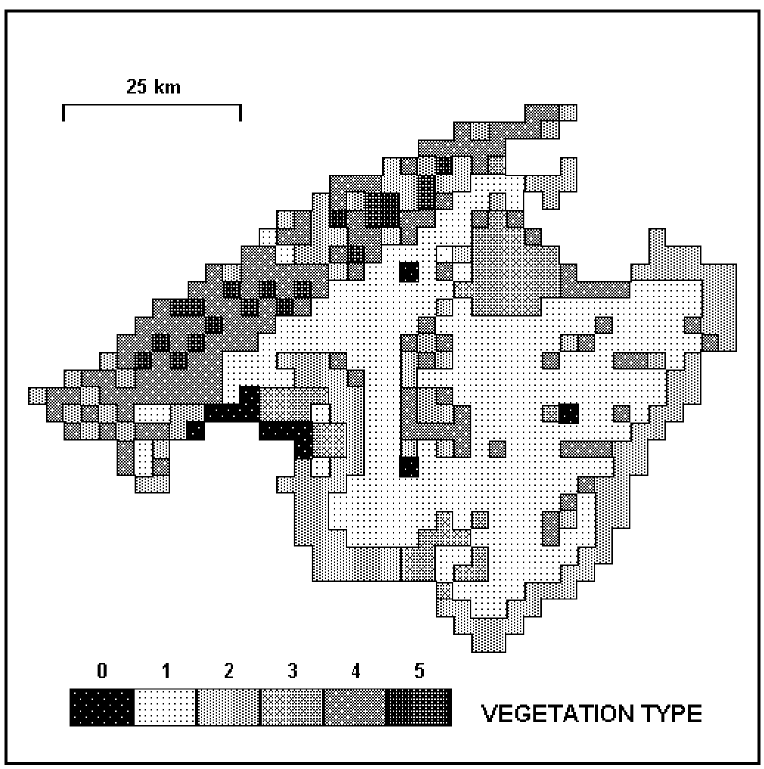

(b)

Figure 4: (a) Soil distribution in Mallorca: 1=sand, 2=sandy loam, 3=silt loam, 4=clay loam and 5=clay; (b) Vegetation distribution: 0=bare, 1=grass, 2=shrub, 3=crop, 4=forest and 5=woodland.

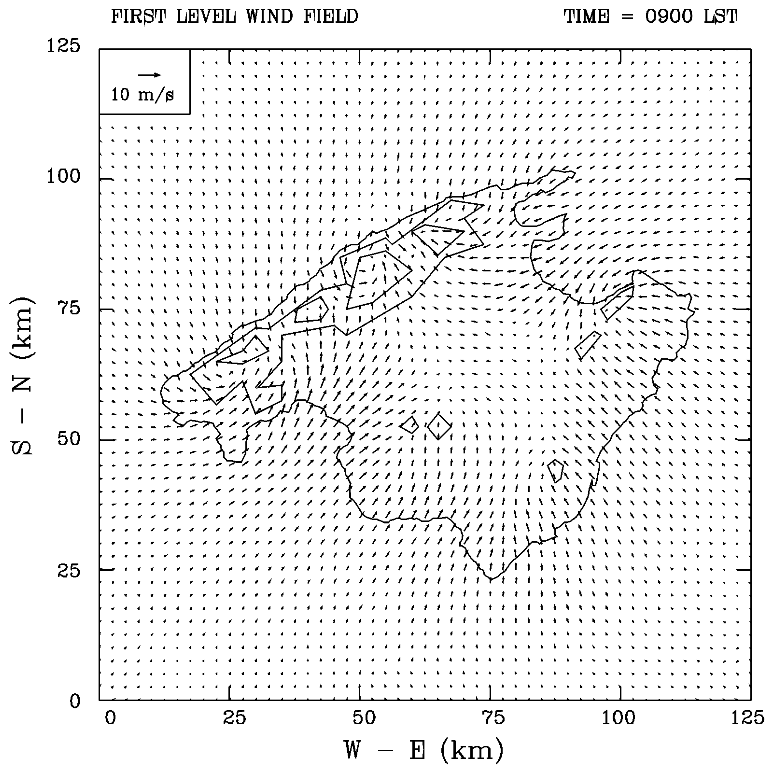

(a)

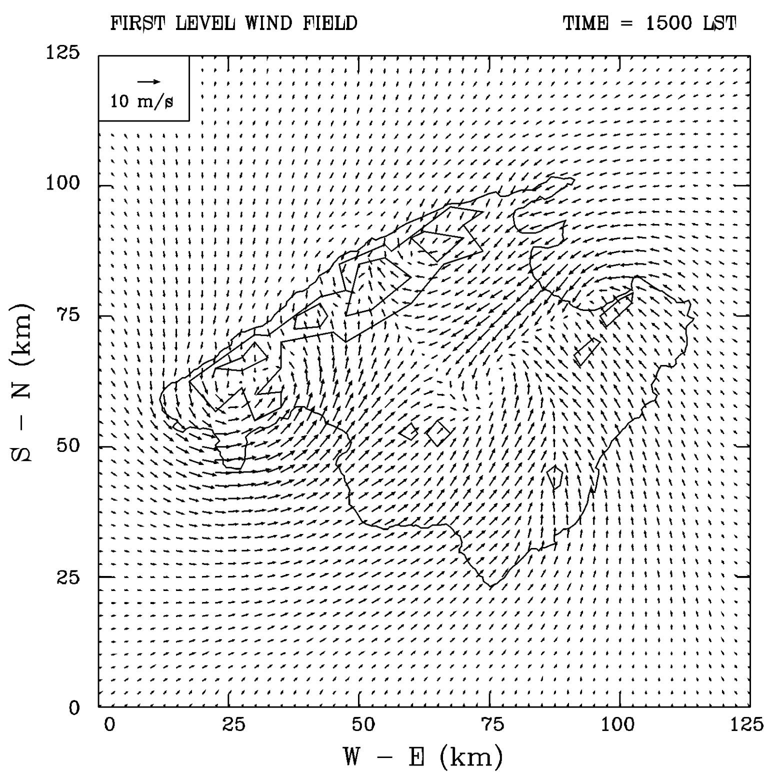

(b)

Figure 5: Simulated sea breeze: (a) at 0900 LST; (b) at 1500 LST; (c) at 2100 LST; (d) at 0500 LST. The arrow on the upper left corner represents 10 $\mathrm{m\,s^{-1}}$. Coastal line and orographic contours of 300 and 700 m are included.

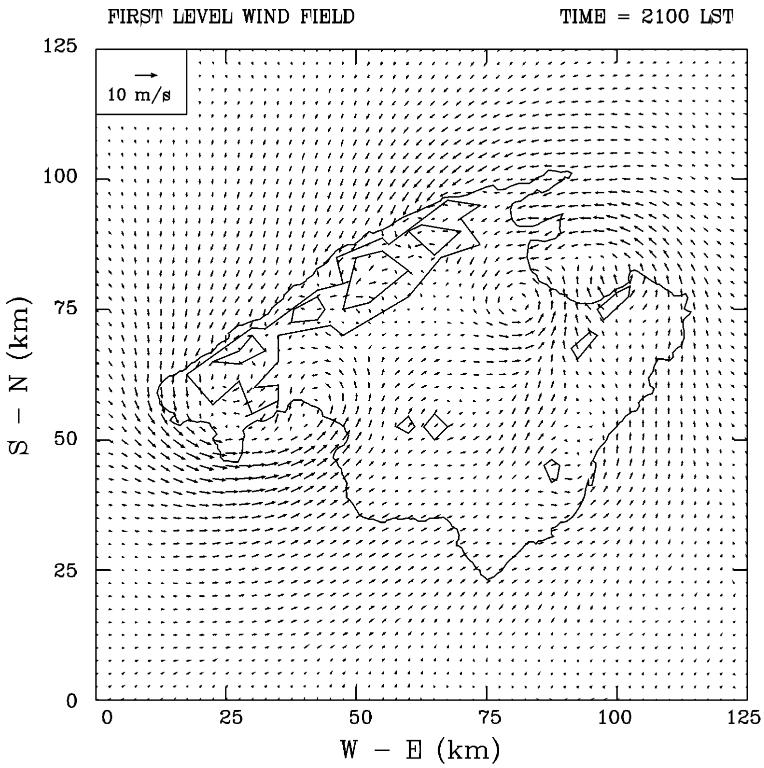

(c)

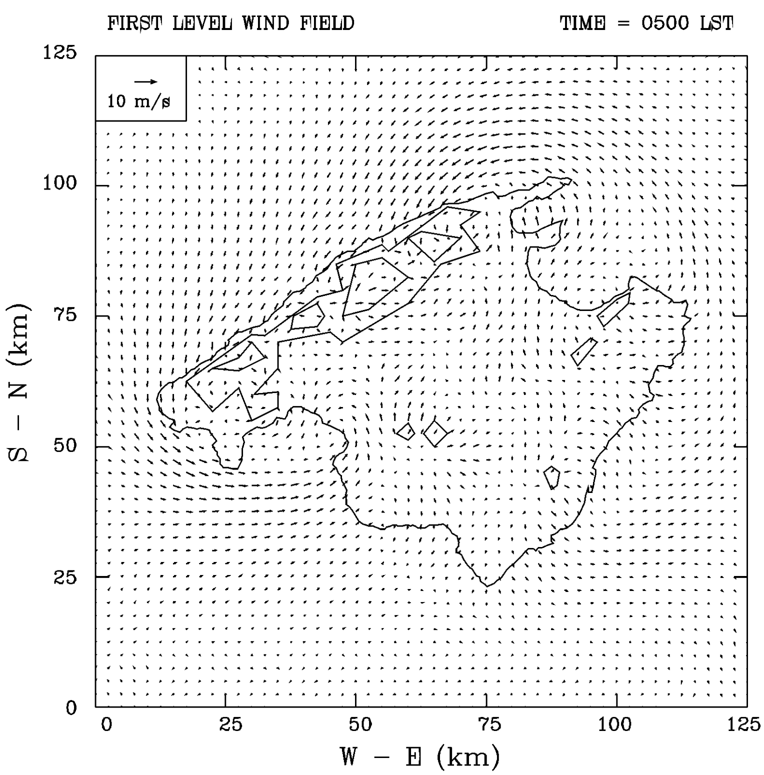

(d)

Figure 5 (cont.).

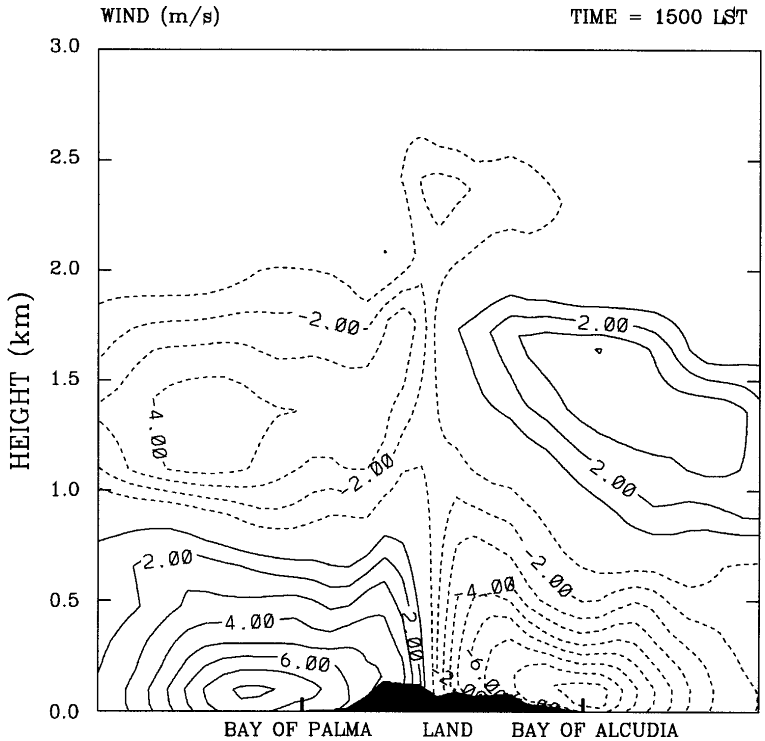

(a)

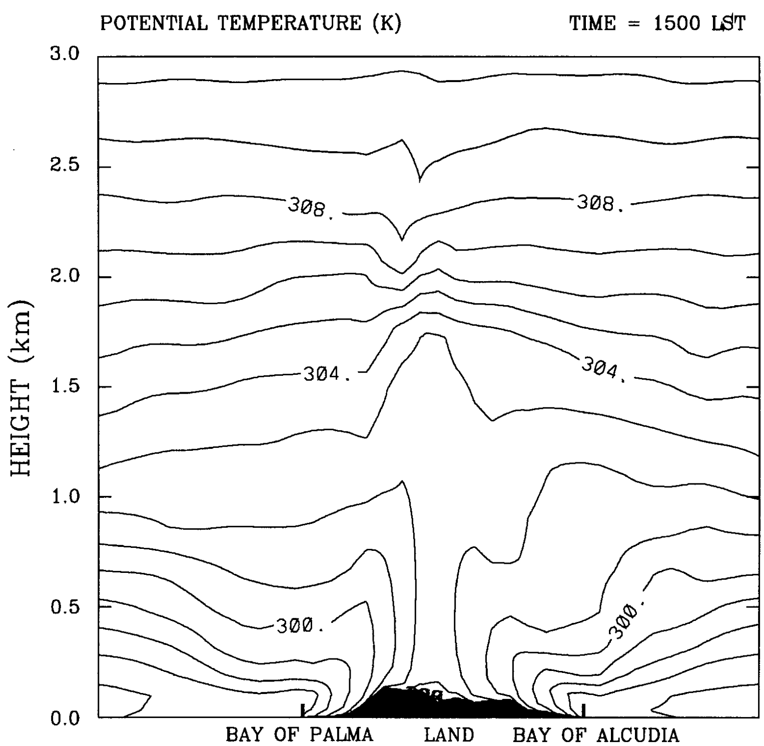

(b)

Figure 6: Vertical cross sections along the bays of Palma and Alcudia: (a) showing the horizontal wind component ($\mathrm{m\,s^{-1}}$) at 1500 LST; (b) showing the potential temperature (K) at 1500 LST (contour interval is 1 K).

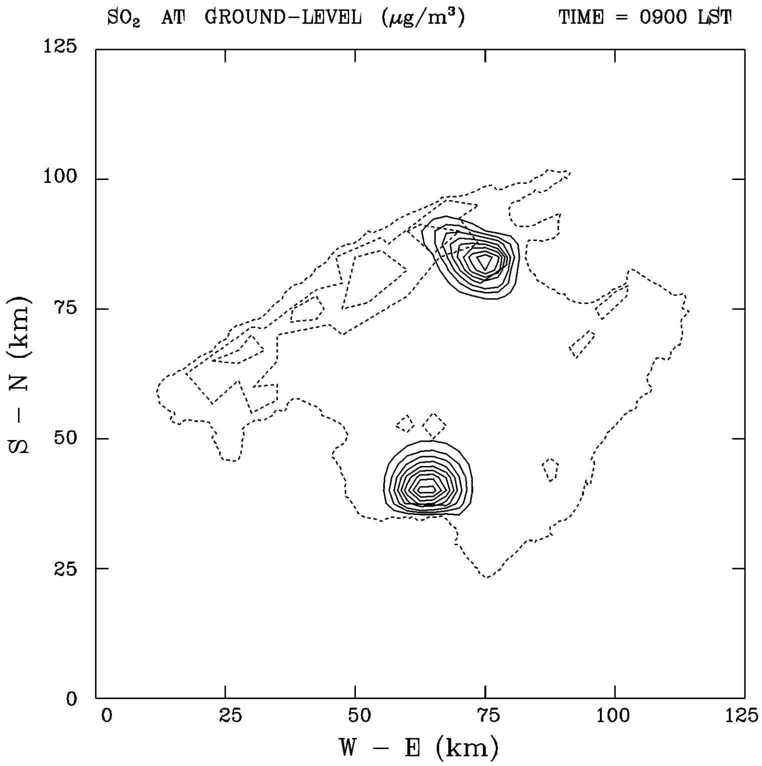

(a)

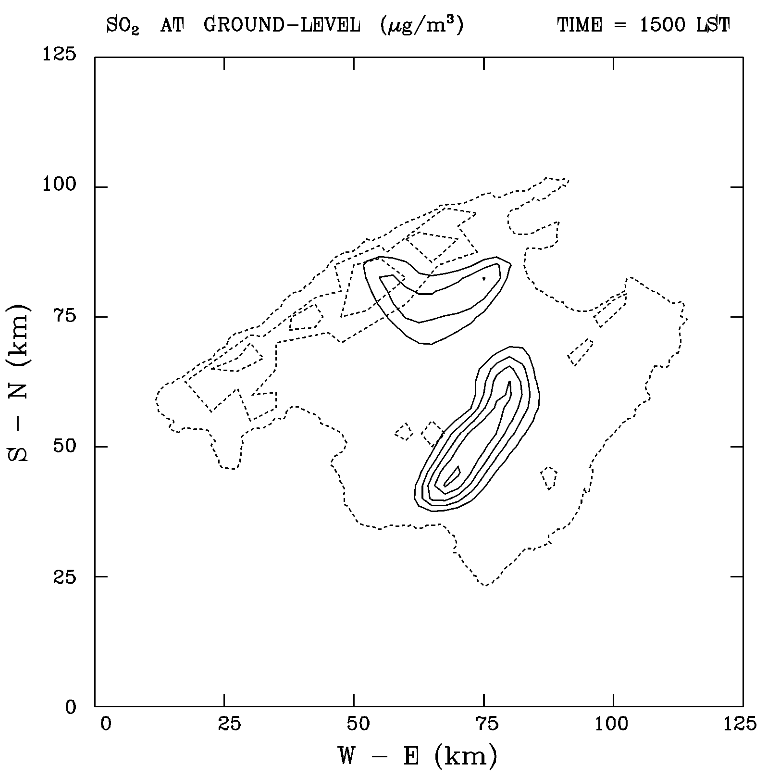

(b)

Figure 7: Results of SO_2 concentration at ground-level for the S2 experiment: (a) at 0900 LST; (b) at 1500 LST; (c) at 2100 LST and (d) at 0500 LST. Contour interval is 5 μg/m^3 starting at 5 μg/m^3 (solid line). Coastal line and orographic contours of 300 and 700 m are also included (dashed line).

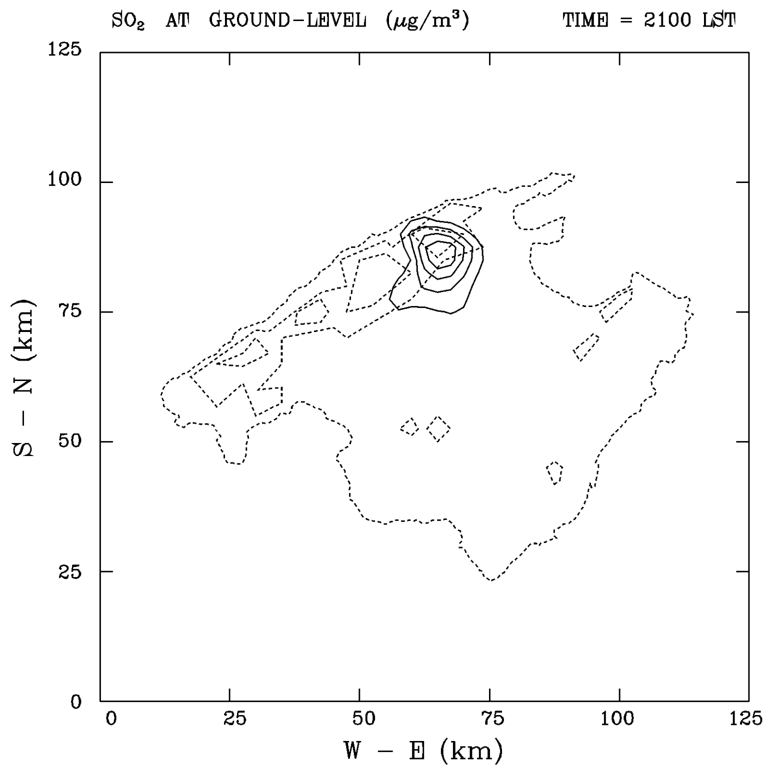

(c)

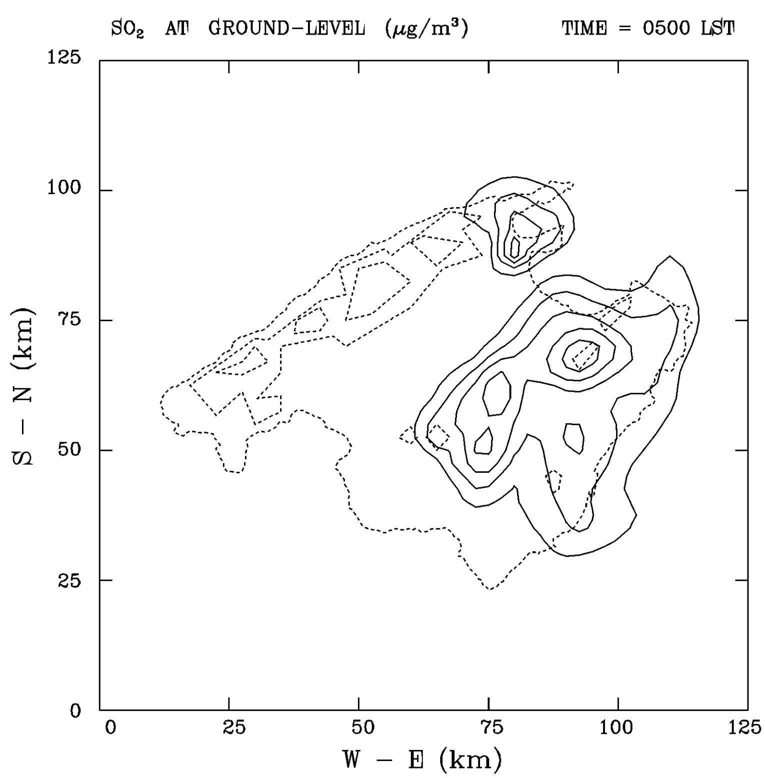

(d)

Figure 7 (cont.).

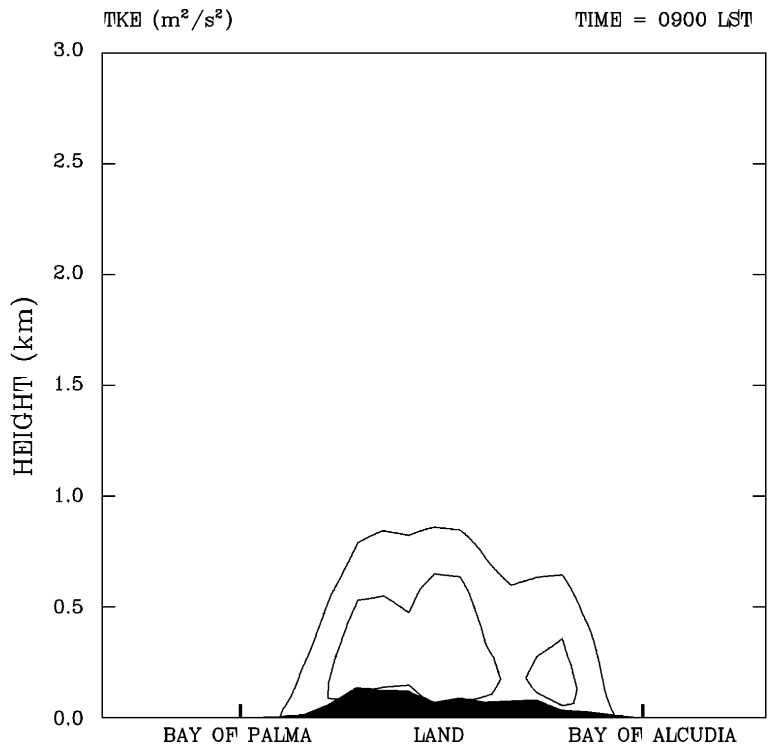

(a)

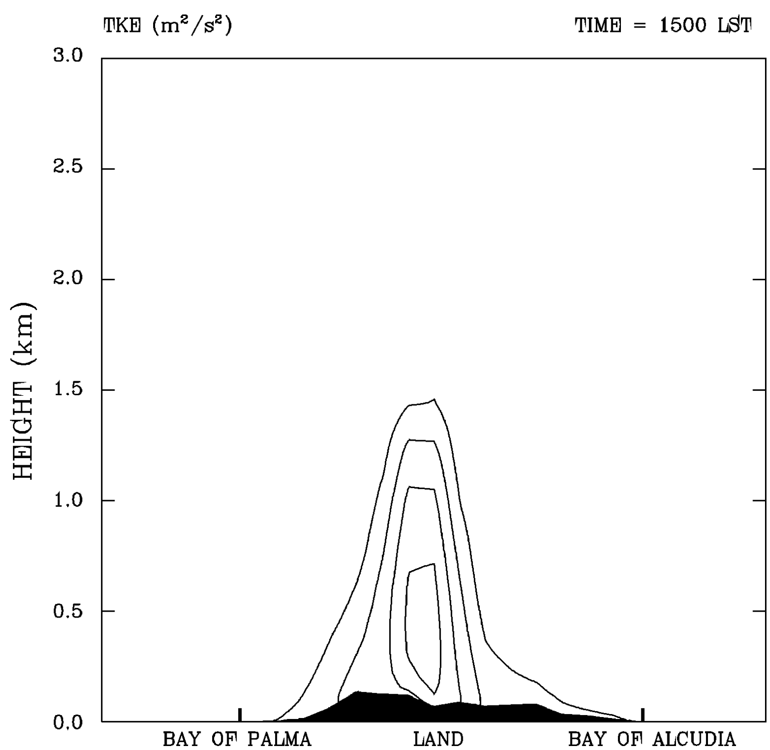

(b)

Figure 8: Vertical cross section along the bays of Palma and Alcudia of the turbulent kinetic energy: (a) at 0900 LST; (b) at 1500 LST. Contour interval is 1 m^2/s^2 starting at 1 m^2/s^2.

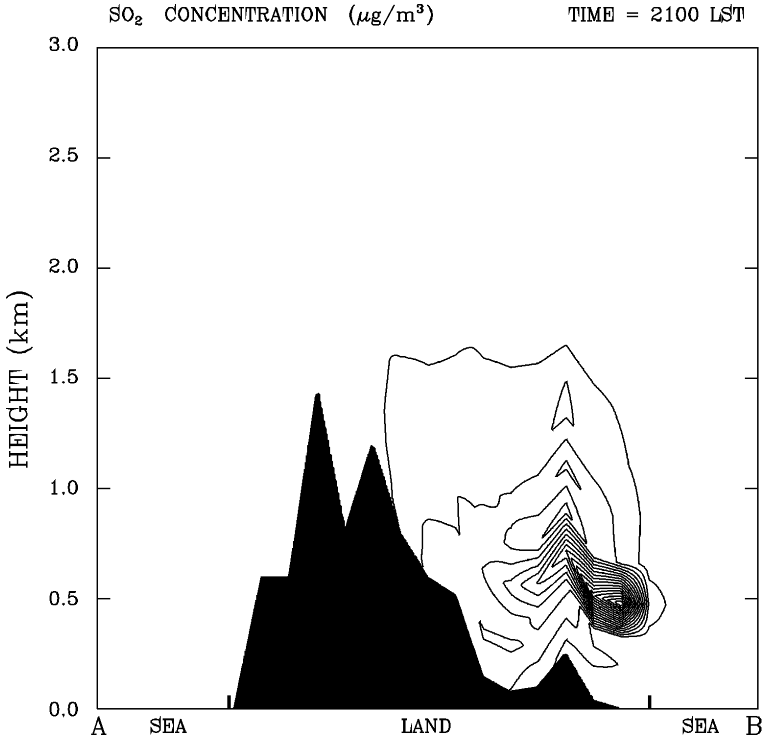

Figure 9: Vertical cross section along AB showing the SO_2 concentration for the S1 experiment at 2100 LST. Contour interval is 10 $\mu g/m^3$ starting at 5 $\mu g/m^3$. Maximum concentration is 165 $\mu g/m^3$.

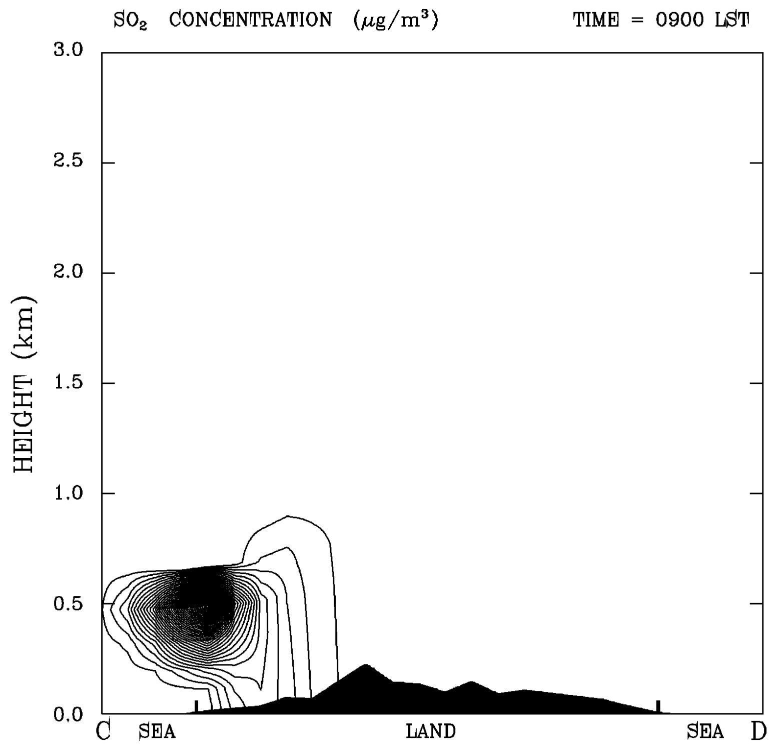

(a)

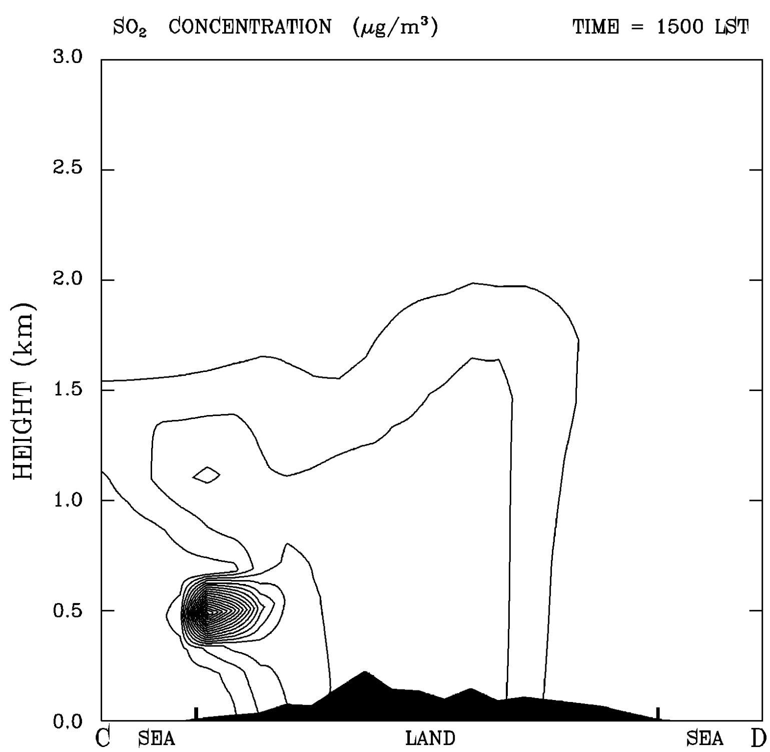

(b)

Figure 10: Vertical cross section along CD showing the SO_2 concentration for the S2 experiment: (a) at 0900 LST, (b) at 1500 LST, (c) at 2100 LST and (d) at 0500 LST. Contour interval is 10 $\mu g/m^3$ starting at 5 $\mu g/m^3$. Maximum concentration is 250, 175, 230 and 235 $\mu g/m^3$ respectively.

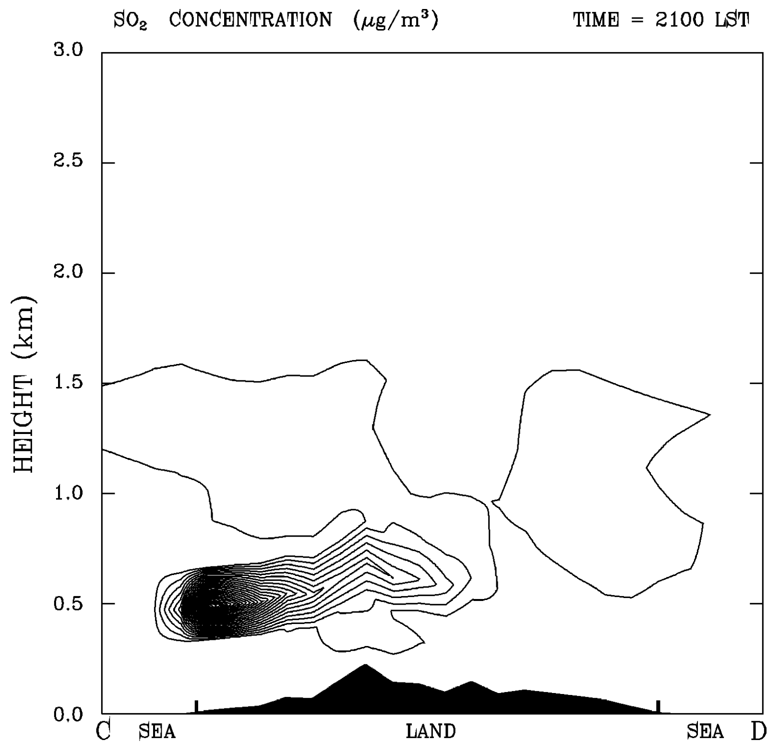

(c)

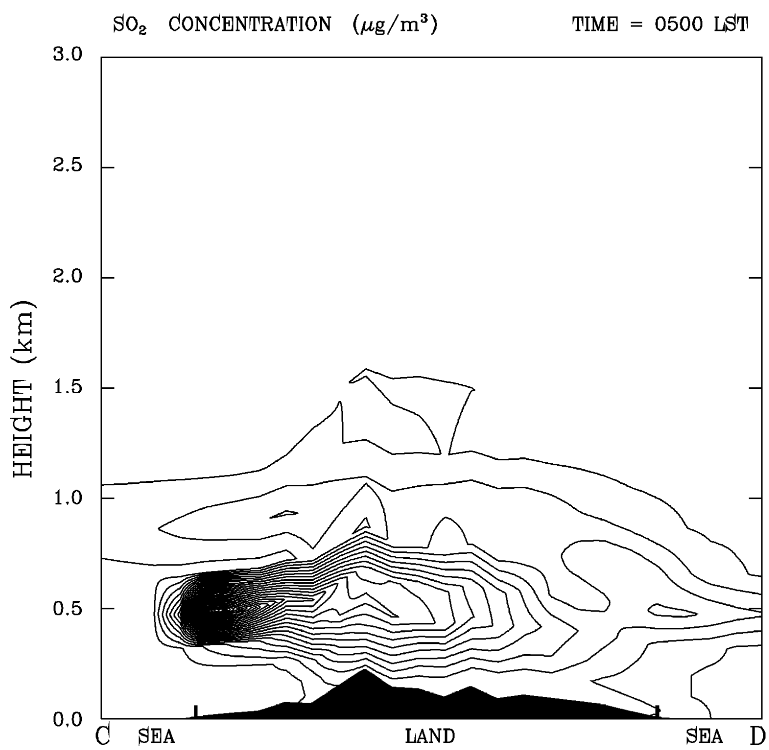

(d)

Figure 10 (cont.).

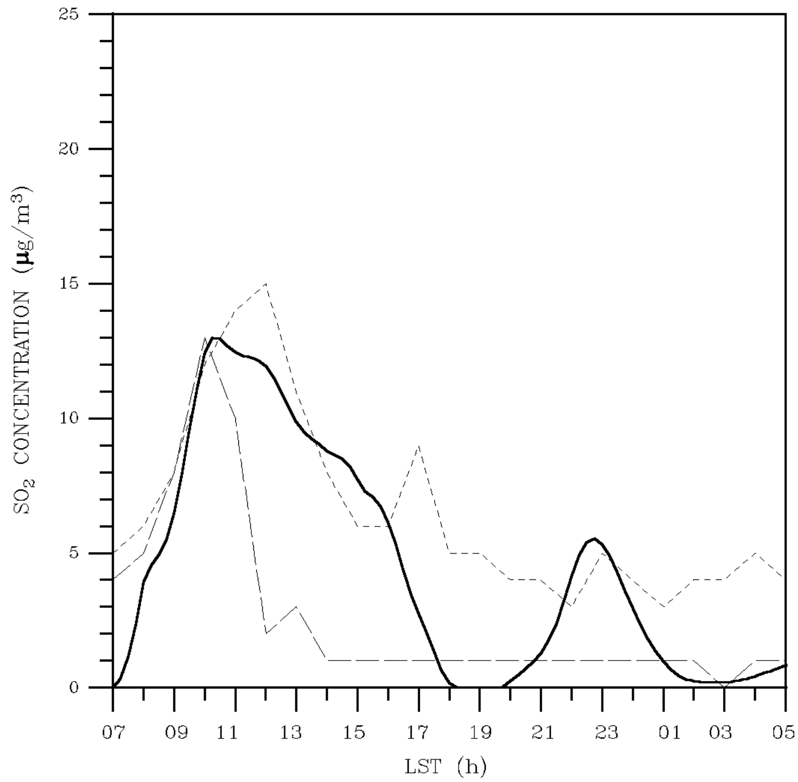

Figure 11: Model results (solid line) compared against measured SO_2 concentrations on 27 July 1993 (short dashes) and 28 July 1993 (long dashes) at IE1.

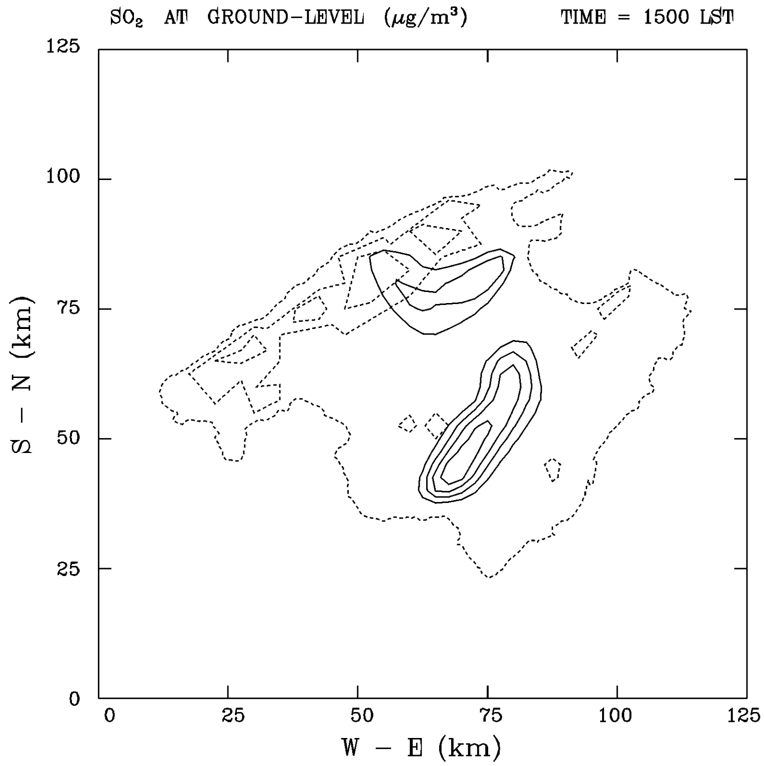

Figure 12: Result of SO_2 concentration at ground-level for the S2 experiment when dry deposition is included. The result corresponds to the first diurnal period at 1500 LST. Contour interval is 5 $\mu g/m^3$ starting at 5 $\mu g/m^3$ (solid line). Coastal line and orographic contours of 300 and 700 m are also included (dashed line).

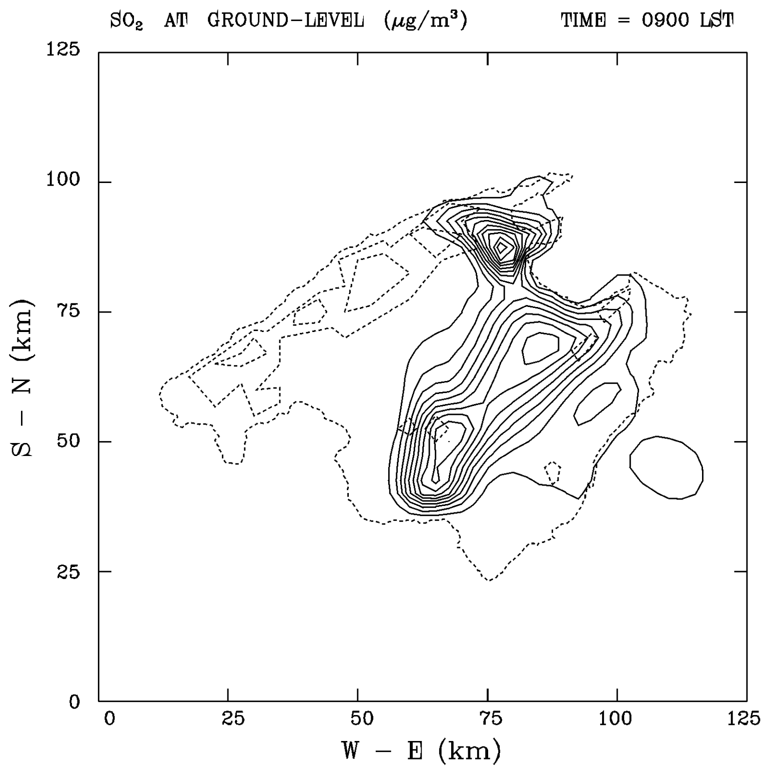

Figure 13: As in Fig. 12 except at 0900 LST of the second diurnal cycle.